Chemical Science

EDGE ARTICLE

View Article Online
View Journal | View Issue

Cite this: *Chem. Sci.*, 2017, **8**, 5930

Using highly emissive and environmentally sensitive *o*-carborane-functionalized metallophosphors to monitor mitochondrial polarity†

Xiang Li,[a] Xiao Tong,[b] Yongheng Yin,[a] Hong Yan,*[a] Changsheng Lu,*[a] Wei Huang[b] and Qiang Zhao*[b]

Mitochondria as vital intracellular organelles play critical roles in multiple physiological processes, and their polarity is a crucial characteristic that can reveal the intracellular environment and impact cellular events. In this work, we designed and synthesized a novel series of highly emissive and environmentally sensitive phosphorescent iridium(III) complexes (**2a–2e**, **3a–3e** and **4**) functionalized by *o*-carborane. These complexes showed high emission quantum yields both in solution and in solid state (up to $\Phi_{PL} = 0.82$), long emission lifetime and tunable emission wavelength over 74 nm by introduction of a carboranyl motif in their ligands. Importantly, all the complexes have shown significant solvatochromic effects in contrast to the carborane-free control complex. Among them, complex **2d** shows the highest sensitivity to polarity of solvents with a MPPS (maximum peak phosphorescence shift) value of 42 nm and clear dependence of phosphorescence lifetime on solvent polarity. Interestingly, complex **2d** can easily penetrate into cells and preferentially distribute in mitochondria. To utilize these properties, the first phosphorescent imaging of mitochondrial polarity has been realized by photoluminescence lifetime imaging microscopy (PLIM), which can monitor mitochondria-relevant cellular processes such as cell apoptosis and distinguish cancer cells from normal cells. Compared to intensity-based sensing, lifetime-based detection is independent of the probe concentration, excitation power and photobleaching of probes, which can show high accuracy and reproducibility.

Received 12th January 2017
Accepted 28th May 2017

DOI: 10.1039/c7sc00160f

rsc.li/chemical-science

Introduction

Polarity plays a crucial role in chemistry and chemical biology, and intracellular polarity reflects a lot of complicated physiological and pathological processes in biological systems. Many cellular events, such as adipogenic differentiation, immune response activation, cell migration and death, and molecular transport across cell layers, may phenotypically lead to polarity variation in cells.[1] Therefore, abnormal changes in polarity are highly relevant to biological disorders and diseases (*e.g.*, diabetes, liver cirrhosis).[2] Mitochondria are vital intracellular organelles and play critical roles in multiple physiological processes, including metabolism, ATP production, cell signaling, and apoptosis. Therefore, mitochondrial polarity assays can reveal information about the cellular internal environment such as transportation of proteins, maintaining of cell function, and homeostasis.[3] Thus it is of great significance to monitor mitochondrial polarity at a cellular level.

Luminescent bioimaging based on optical probes is a powerful technique for monitoring cellular environmental processing in living systems and has received considerable interest in recent years.[4] Currently, some polarity-sensitive fluorescent probes are available.[3,5] However, those fluorescent probes are mainly limited to organic dyes, which feature short emission lifetime and suffer from background interference from biosamples and serious photobleaching.[6] In contrast, the phosphorescent transition-metal complexes (PTMCs, namely metallophosphors), especially the iridium(III) complexes, exhibit advantageous photophysical properties, such as long phosphorescence lifetime as well as high quantum yield and excellent photostability. These make them promising probes for biological imaging. Especially, their long and sensitive phosphorescence lifetimes are very beneficial for lifetime-based biosensing and bioimaging by photoluminescence lifetime imaging microscopy (PLIM), which can effectively eliminate the unwanted background interference based on the emission lifetime difference between the phosphorescent probe and interference signal. Moreover, the emission lifetime as the

[a]*State Key Laboratory of Coordination Chemistry, School of Chemistry and Chemical Engineering, Nanjing University, Nanjing 210023, P. R. China. E-mail: hyan1965@nju.edu.cn; luchsh@nju.edu.cn*

[b]*Key Laboratory for Organic Electronics & Information Displays, Institute of Advanced Materials, Nanjing University of Posts and Telecommunications, Nanjing 210023, P. R. China. E-mail: iamqzhao@njupt.edu.cn*

† Electronic supplementary information (ESI) available: Details of synthesis and spectra data, biological studies and tables. CCDC 1496512–1496520. For ESI and crystallographic data in CIF or other electronic format see DOI: 10.1039/c7sc00160f

sensing signal is independent of the probe concentration, excitation power and photobleaching of probes, which can show high accuracy and reproducibility.[7] To date, there have been no reports about polarity-sensitive phosphorescent probes for bioimaging. Therefore, the development of a new type of phosphorescent probes through a combination of high quantum yield, long emission lifetime and excellent polarity sensitivity is highly desired.

Icosahedral *o*-carborane ($1,2\text{-}C_2B_{10}H_{12}$) possesses strong electron-withdrawing ability (C-substitution) and an alterable C–C bond.[8] *o*-Carborane cage can serve as a rigid hindrance to prevent probable intermolecular interactions and reduce self-quenching as well as potential concentration quenching.[9] Its electron-withdrawing ability can lead to considerable charge redistribution of the phosphorescent core, which can further result in a large emission shift.[10] On the other hand, the stretchable C–C bond is quite sensitive to its chemical surroundings, such as substitution at the C–H bonds[8–10] and even solvents or media.[10] From this viewpoint, *o*-carborane embedded metallophosphors might be an ideal polarity-sensitive probe in cell imaging for potential biomedical applications.

On the basis of the above hypotheses, a novel series of phosphorescent iridium(III) complexes based on *o*-carborane functionalized N^N ligands have been designed and synthesized for the first time (Scheme 1). The introduction of carborane to the bipyridine ligand of the cationic iridium(III) complexes (**2a–2e**, **3a–3e** and **4**) has led to highly improved phosphorescence quantum yields both in solution (from 0.26 to 0.79) and in solid state (from 0.07 to 0.82) in comparison to the carborane-free control complex **Model**. The emission color has been tuned from green to yellow, or even to red (up to 74 nm). The photophysical properties of these iridium(III) complexes are quite sensitive to the polarity of solvents. Interestingly, the complexes show mitochondria targeting, therefore complex **2d** was chosen to develop a phosphorescence probe for monitoring mitochondrial polarity at the cell level through photoluminescence lifetime imaging microscopy. As a result, such a probe can distinguish cancer cells from normal cells, as well as differentiate living cells from dying cells and dead cells.

Results and discussion

Synthesis and characterizations

The novel *o*-carborane-modified N^N ligands (**1a–1j**) (Schemes 1 and S1†) were synthesized in high yields by using commercially available $B_{10}H_{10}(Et_4N)_2$ which is cheap, stable and non-toxic.[9f] Through the change of the 2-R substituent or the substitution site of the carboranyl unit at bipyridine,[11,12] two series of complexes **2a–2e** and **3a–3e** were prepared by the reactions of the dimeric $[(C^N)_2Ir(\mu\text{-}Cl)_2Ir(C^N)_2]$ and the corresponding carborane-functionalized ligands (**1a–1j**) (Schemes 1 and 2). Complex **4** containing two carboranyl motifs was also synthesized in order to further tune the photophysical properties. Both the new ligands and the newly generated iridium(III) complexes have been fully characterized by NMR, MS spectroscopy, elemental analyses, and X-ray diffraction (Fig. 1, S1 and Table S1†). The crystal structures of complexes **Model**, **2a**, **2b**, **2d**, **3b**, **3c**, and **3e** exhibit a distorted octahedron geometry around the iridium center (Fig. 1), and the carboranyl units have led to an obvious increase in the volume of the complexes (Tables S1 and S2†). Due to the bulkiness of *o*-carborane, no intermolecular π–π interactions were observed from the packing structures. The advantage of the bulky carborane cage in inhibiting intermolecular interactions is important to improve the

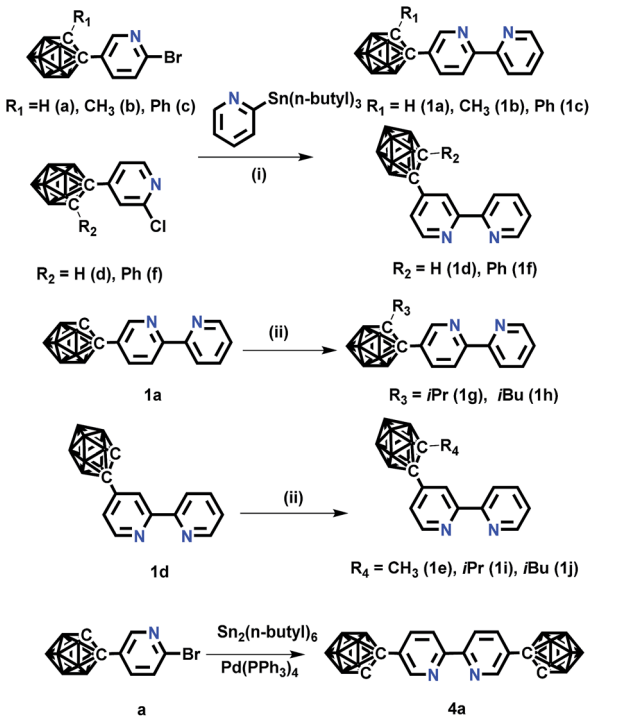

Scheme 1 The synthetic routes of *o*-carborane modified N^N ligands. Conditions: (i) $Pd(PPh_3)_4$, toluene, 110 °C, 24 h; (ii) NaH, RI (R = CH_3, iPr, iBu), DMF, −20 °C.

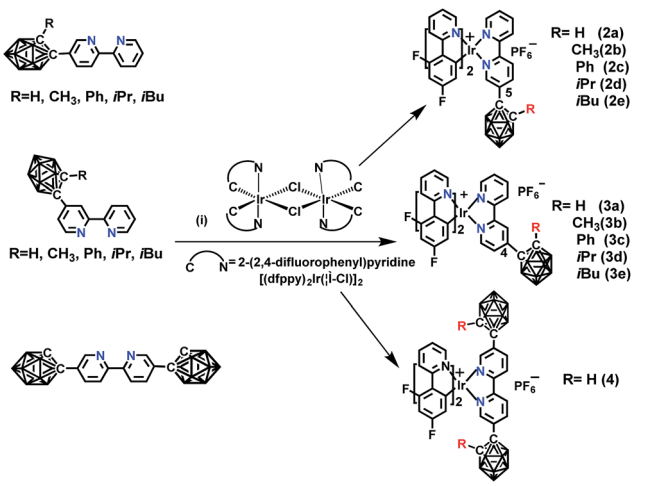

Scheme 2 The synthetic routes of *o*-carborane modified iridium(III) complexes: (i) CH_2Cl_2/CH_3OH (1 : 1, v/v), refluxing overnight, KPF_6.

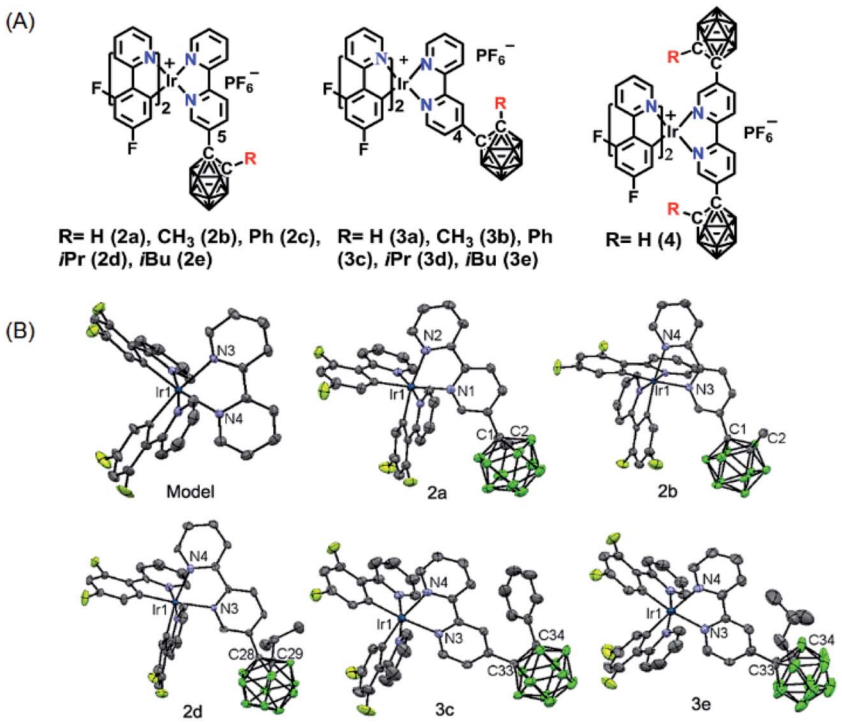

Fig. 1 (A) Nomenclatures of carborane-modified iridium(III) complexes; (B) ORTEP diagrams of complexes **Model**, **2a**, **2b**, **2d**, **3c**, and **3e**. H atoms, solvent molecules, and PF_6^- anions are omitted for clarity.

phosphorescent emission of iridium(III) complexes both in solution and in solid state.

Photophysical properties

The UV/vis absorption and photoluminescence (PL) spectra were measured in CH_2Cl_2 solution (Table 1). All the complexes show similar absorption bands (Fig. S10 and S11†) compared to the model one. The main strong absorption bands below 350 nm are mainly attributed to the π–π* transitions from the ligands. The weak absorption bands from 350 nm to 450 nm are assigned to metal-to-ligand charge transfer (MLCT) and ligand-to-ligand charge transfer (LLCT) characters, which is referenced by the similar reported ionic iridium(III) complexes. In solution, **2a–2e** have similar emission wavelength ($\lambda = 563$ nm) (Fig. 2(A)), but a 43 nm bathochromic shift was observed in comparison to the **Model**, corresponding to the emission color change from green to yellow. The quantum yields have been improved varying from 0.49 to 0.79 (referenced to 0.26 for the **Model**, see Table 1) dependent on the 2-R substituent at *o*-carborane, which is higher than the cationic iridium complex ($\Phi_{PL} = 0.67$) containing *o*-carborane modified cyclometalated ligands.[9d] The highest quantum yield was observed as 0.79 for **2d** owing to the relatively large size of the R (iPr) group. Complexes **3a–3e**

Table 1 Photophysical and electrochemical data of iridium(III) complexes

Complex	λ_{abs}[a] [nm] (lg ε)	λ_{em}[a] [nm]	τ[b] [ns]	Φ_{PL}[b]	E^{ox}_{onset} (eV)	E_g[c] (eV)	HOMO/LUMO[b] (eV)
2a	244(4.0), 296(3.7), 309(3.7), 364(2.9)	563.0	1115.0	0.49(0.41)	1.239	2.94	−6.039/−3.049
2b	251(4.0), 300(3.8), 315(3.8), 365(3.1)	563.0	746.9	0.59(0.37)	1.251	2.95	−6.051/−3.101
2c	246(4.2), 303(3.9), 315(3.9), 362(3.3)	560.0	794.0	0.62(0.16)	1.270	2.95	−6.070/−3.120
2d	246(4.1), 304(3.9), 315(3.9), 363(3.3)	563.0	760.0	0.79(0.82)	1.257	2.96	−6.057/−3.097
2e	246(4.1), 304(3.8), 314(3.8), 362(3.3)	563.0	774.6	0.72(0.63)	1.259	2.97	−6.059/−3.087
Model	247(4.0), 303(3.8), 316(3.8), 362(3.1)	520.0	561.5	0.26(0.07)	1.208	3.18	−6.008/−2.828
3a	244(4.1), 298(3.8), 315(3.8), 362(3.4)	555.0	585.3	0.55(0.49)	1.225	2.99	−6.025/−3.039
3b	246(4.1), 299(3.8), 315(3.7), 362(3.3)	555.0	733.0	0.66(0.67)	1.240	2.99	−6.040/−3.053
3c	266(4.0), 298(3.8), 317(3.7), 363(3.3)	553.0	465.1	0.68(0.54)	1.238	2.99	−6.038/−3.048
3d	243(4.2), 304(3.9), 315(3.8), 361(3.5)	556.0	759.3	0.76(0.49)	1.228	2.98	−6.028/−3.046
3e	244(4.1), 303(3.8), 314(3.8), 361(3.4)	556.0	793.6	0.73(0.71)	1.232	2.98	−6.032/−3.050
4	249(2.4), 311(3.7), 321(3.8), 364(3.3)	594.0	597.5	0.33(0.18)	1.260	2.81	−6.060/−3.252

[a] In CH_2Cl_2. [b] Data in degassed CH_2Cl_2 at 298 K (1.0×10^{-5} M) and data measured in solid state are given in parentheses. [c] HOMO (eV) = $-e(E^{ox}_{onset} + 4.8)$, $E_g = 1240/\lambda$, LUMO (eV) = E_g + HOMO.

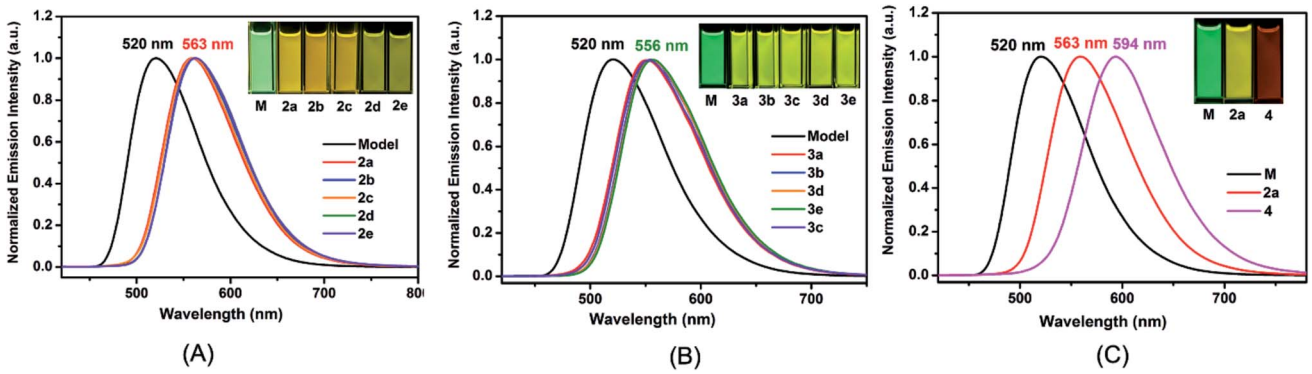

Fig. 2 PL spectra of iridium(III) complexes: (A) complexes **2a**, **2b**, **2c**, **2d**, **2e**, and **Model**; (B) complexes **3a**, **3b**, **3c**, **3d**, **3e**, and **Model** in degassed CH_2Cl_2 (1.0×10^{-5} M) at room temperature. (C) PL spectra of iridium(III) complexes **Model**, **2a**, and **4** in degassed CH_2Cl_2 (1.0×10^{-5} M) at room temperature ($\lambda_{ex} = 365$ nm and corresponding luminescence photographs are inset).

containing an *o*-carboranyl unit at a different site of the N^N ligand also show highly efficient emission in solution (Φ_{PL} = 0.55–0.76, Table 1). Their emission wavelength is positioned at 556 nm (Fig. 2(B)), having a 36 nm bathochromic shift compared to the **Model**. A significant red shift of 74 nm has been achieved in complex **4** (594 nm in Fig. 2(C)). Obviously, this is attributed to the cooperative electron-withdrawing property of the two-carboranyl motifs. But the quantum yield of **4** (0.33) in solution has little increase in comparison to the **Model** (0.26), which may be attributed to the "energy gap law".[13] It is worthy to note that the solid-state quantum yields of these iridium(III) complexes are also significantly increased from 0.07 for **Model** to 0.16–0.82 for **2a–2e** and 0.49–0.71 for **3a–3e**, respectively (Table 1 and Fig. S12†), which are among the highest values for metallophosphors. The bulkiness of carborane cage has played an important role in inhibiting intermolecular interactions (Fig. S2–S9†) as indicated by the longer Ir–Ir distances along one or more axes between adjacent metal centers in comparison to the model complex (Fig. S2–S9†). In addition, 2-R substituents decrease the flexibility of molecular structures and increase the volumes of the corresponding unit cells (Tables S1 and S2†), which are important to suppress the interactions between metallophosphors and improve quantum yields. This is clearly attributed to the steric property of the carboranyl motif.

Cyclic voltammograms and DFT calculations

The electrochemical studies have revealed that all the complexes have reversible oxidation waves with potentials in the range of 1.2–1.3 V (Fig. S13† and Table 1). The oxidation potentials of **2a–2e** are similar, independent of the 2-R substituent at the *o*-carboranyl unit. The same occurs for **3a–3e**. This is consistent with the energy gaps and emissive wavelengths. DFT calculations (Fig. S20–S22†) have shown that all the 2-R substituents at carborane are not involved in orbitals, indicating no contribution to the energy levels.[14] The HOMOs are mostly distributed over the cyclometalated C^N ligands. The LUMOs of complex **Model** are distributed merely on the bipyridine ligand, whereas those of carborane-embedded complexes are mainly located on bipyridine plus a small fraction on the carboranyl motif. Owing to the inductive electron-withdrawing effect of carborane, the HOMO − LUMO energy gaps of **2a–2e** are narrowed by about 0.23 eV because of the greater LUMO stabilization than that of HOMO, in comparison to the narrowed values of about 0.19 eV for **3a–3e** (Fig. S20 and S21†). The LUMO level in complex **4** has been further decreased, demonstrating the overlaid inductive electronic effect of the two carboranyl groups. Thus, the DFT calculations are consistent with the observed red-shifted emissions.

Solvatochromic effect

Interestingly, all the complexes have shown significant solvatochromic effects in contrast to complex **Model**. The maximum peak phosphorescence shift (MPPS, denoted as $\Delta\nu$), is defined as the maximum difference between emissions in the low polar solvent toluene (0.36 debye) and in the high polar solvent DMSO (3.96 debye).[15] Thus $\Delta\nu$ is given as 9 nm for **Model**, 19 nm for **2a**, 32 nm for **2b**, 34 nm for **2c**, 42 nm for **2d**, 18 nm for **2e**, 7 nm for **3a**, 7 nm for **3b**, 24 nm for **3c**, 21 nm for **3d**, 6 nm for **3e**, and 27 nm for **4** (Fig. S14–S19 and Table S3†). Among them, complex **2d** exhibits the largest MPPS of 42 nm, corresponding to a distinct color change from green to yellow (Fig. 3(A)). The emission intensity and lifetime of complex **2d** show a decreasing trend with the increase of solvent polarity (Fig. S26†).

Studies on MLCT (metal to ligand charge transfer) in iridium(III) complexes have revealed that the solvatochromic effect is related to molecular dipole moments.[15] Thus the singlet (S_0) and triplet (T_1) dipole moments of the complexes in different solvents were calculated (Tables S4 and S5†), and the transition dipole moments (ΔT_1–S_0) are summarized in Fig. 4 and Tables S6 and S7.† Complexes **2c**, **2d**, and **3c** show big (ΔT_1–S_0) changes from those in toluene to those in DMSO. This is in accordance with the MPPS shown in emissions (*i.e.* 34 nm for **2c**, 42 nm for **2d**, and 24 nm for **3c**). Generally, introduction of the electron-withdrawing carboranyl group into the bipyridine ring (N^N ligand) has enhanced the transition dipole moments in comparison to complex **Model** (Tables S6 and S7†). The

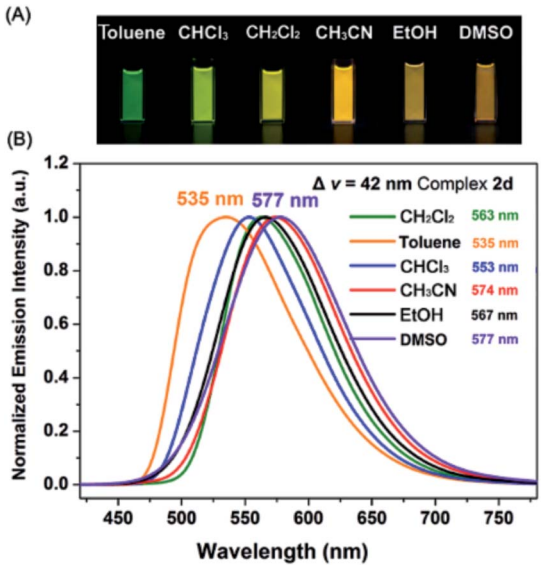

Fig. 3 (A) Luminescence photographs of **2d** in various solvents. (B) Phosphorescence spectra of complex **2d** in toluene (0.36 D), chloroform (1.04 D), dichloromethane (1.60 D), acetonitrile (3.84 D), ethanol (1.69 D), and DMSO (3.96 D).

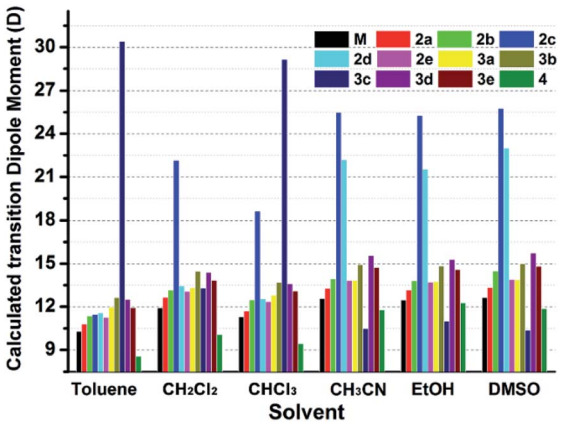

Fig. 4 Calculated transition dipole moments (ΔT_1–S_0) of iridium complexes in different solvents (see data in Tables S7 and S8†).

calculations also demonstrate that the molecular transition dipole moments of the iridium(III) complexes can be finely adjusted by the carboranyl group, as reflected by different emissions. This might shed new light on the utilization of the transition dipole moments of iridium(III) complexes for applications.

Cell imaging

Complex **2d** shows high quantum yields both in solution (Φ_{PL} = 0.79) and in solid state (Φ_{PL} = 0.82) as well as sensitive emission color and lifetime toward solvent polarity. Therefore, it might be a potential polarity probe by the PLIM technique. As such, the phosphorescent emission in pH 4–10 was measured, which showed no change (Fig. S23†). Next, **2d** was found to be more photostable in comparison to the commercially available reference (Mito-Tracker-Red) (Fig. S24†). Moreover, the phosphorescence intensity of **2d** was little affected in the presence of common metal ions (Na^+, K^+: 5 mM; Ca^{2+}, Mg^{2+}: 500 μM; Zn^{2+}, Al^{3+}, Mn^{2+}: 200 μM) and various reactive oxygen species (H_2O_2: 50 μM; ClO^-, O_2^-, ·OH: 100 μM) (Fig. S25 and S26†). Also, the emission intensity changes little with increasing viscosity from 0.60 cP to 100 cP (Fig. S27†).

An MTT assay has shown that complex **2d** exhibits no cytotoxicity towards HepG2 cells at concentrations under 10 μM, thus making it suitable for cellular staining experiments (Fig. S28†). Colocalization imaging experiments were performed for liver human hepatoma cells (HepG2) and normal human liver cells (HL-7702) with complex **2d** and Mito Tracker Red (mitochondrial dye) to demonstrate that complex **2d** can readily penetrate into cells (Fig. S29†). More importantly, complex **2d** showed mitochondria targeting with Pearson's colocalization coefficients of 0.96 and 0.90 in the two cell lines, respectively. It is likely that A549 and HeLa cells also showed mitochondria targeting (Fig. S29†). Other subcellular organelle staining control experiments gave the colocalization coefficients 0.18 for Lyso (lysosomes), 0.68 for Golgi apparatus, 0.72 for ER (endoplasmic reticulum) (Fig. S30†). These experiments further demonstrate that complex **2d** can preferentially accumulate in mitochondria. This is probably attributed to its cationic charge and lipophilic carboranyl group[3,5] since complex **2d** is independent of mitochondrial membrane potential as indicated by the fact that both emission intensity and lifetime of the complex were almost unchanged in the absence or presence of CCCP (carbonyl cyanide 3-chlorophenylhydrazone) (Fig. S31†).

It is well known that cancer cells have different microenvironments from normal cells. In many cases, cancer cells have exhibited mitochondrial disorders. Therefore, we intended to detect the polarity difference in mitochondria in different cell lines by using complex **2d** and the PLIM technique. In doing so, the emission spectrum of complex **2d** within the cells was measured and was found to be nearly identical to that observed in the extracellular environment (Fig. S32†). The phosphorescence lifetime was also examined and found not to be affected by the dosage of **2d** (10, 20, and 30 μM), demonstrating that the probe is stable during cellular imaging (Fig. S33†). Next, HepG2 and HL-7702 cells were incubated with complex **2d** (10 μM). The emission lifetime and phosphorescence intensity in HepG2 cells were observed to be much longer and higher than those in HL-7702 cells (Fig. 5(A)).

According to the polarity–lifetime relationship (Fig. S34†), the cellular environment of HepG2 cells is less polar than that of normal cells (HL-7702), consistent with the reported result.[3,4,5a] In contrast, HeLa and A549 cell lines exhibited little difference in phosphorescence lifetime in comparison to HL-7702 (Fig. 5(A) and S34†). In particular, both the emission lifetime and phosphorescence intensity of **Model** remained almost the same in HL-7702 cells, HepG2, A549, and HeLa cell lines (Fig. S35†), indicating insensitivity toward polarity within cells. Hence, the PLIM results demonstrate that complex **2d** can be used as a phosphorescent probe to detect the mitochondrial polarity in live cells.

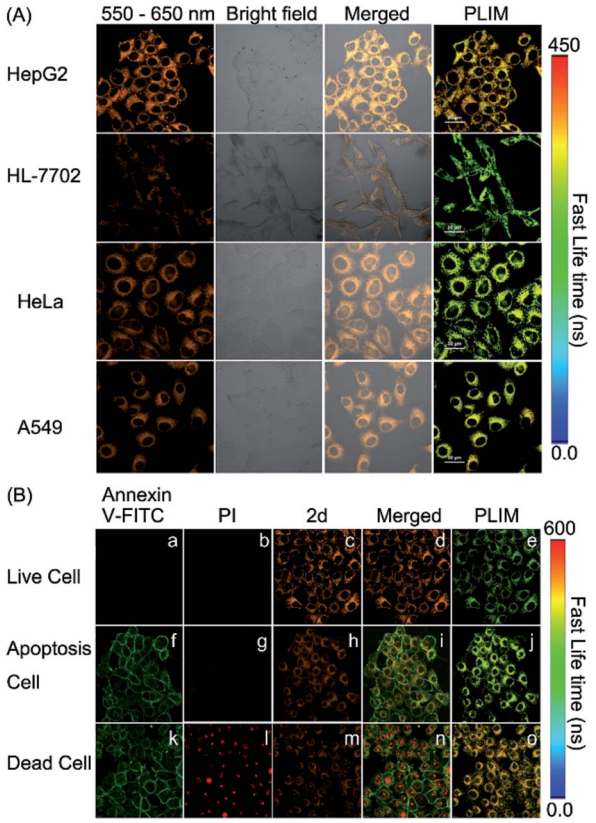

Fig. 5 (A) Phosphorescence lifetime imaging of the mitochondrial polarity in HepG2, HL-7702, HeLa, and A549 cells stained with **2d** (10 μM) (scale bar: 30 μm). (B) Phosphorescence lifetime imaging of HepG2 cells in different states stained with **2d** (10 μM).

Mitochondrial disorders are well-known to be highly relevant to apoptosis, which is basically defined as a programmed cell-death event in contrast to the unprogrammed cancer cell growing.[16,17] During apoptosis process, mitochondria change both in structure and in function.[17] Hence, we tried to further use PLIM to monitor the change of mitochondrial polarity during cell apoptosis. Complex **2d** and the commercial dye propidium iodide (PI), or Annexin-FITC were incubated together with live HepG2 cells, cells in apoptosis and dead cells, respectively. As illustrated in Fig. 5(B), the emission lifetimes in cells in different states vary. The PLIM signals in living cells show the shortest phosphorescence lifetime, whereas those for dead cells exhibit the longest phosphorescence lifetime. In a sharp contrast, the control **Model** complex has indicated almost zero-difference in the PLIM signals during cell apoptosis (Fig. S36†). Therefore, the PLIM technique clearly indicates polarity decreasing in mitochondria during cell apoptosis through the use of the phosphorescent probe complex **2d**, which can unambiguously differentiate live, apoptotic, and dead cells.

Conclusions

In summary, a novel series of highly emissive phosphorescent iridium(III) complexes containing *o*-carborane modified N^N ligands have been designed and synthesized. Among them, an efficient polarity-sensitive phosphorescent probe (complex **2d**) has been developed for the first time. It exhibits a visual color change of phosphorescence emission as a function of polarity and unique mitochondria affinity. This cell-staining complex has shown the ability to discriminate cancer cells and normal cells by PLIM. Moreover, this phosphorescence probe can be used to track cell apoptosis to indicate living cells, cells in apoptosis, and dead cells. Hopefully, this new type of *o*-carborane-functionalized phosphorescent probe could be further improved to detect mitochondrial disorders in the future.

Experimental

General

In this paper, all the synthetic steps were carried out under an inert argon atmosphere using standard Schlenk and glovebox techniques unless otherwise noted. Commercial reagents were used without any further purification. All the solvents are freshly distilled, for example, THF and toluene were distilled on sodium/benzophenone as well as acetonitrile and EtOH on CaH_2. Dimeric $[(C^N)_2Ir(\mu\text{-}Cl)]_2$ complex was prepared by literature procedures.[S1]† Intermediate compound $B_{10}H_{12}(Et_2S)_2$ was synthesized by a modified method according to literature reports.[S2,S3a]† Compounds **a**,[S3a]† **b**,[S3a]† **11c**,[S3b]† **11d**,[S3c]† and **11f**[S3b]† were synthesized according to the literature. All NMR spectra (^{1}H-, ^{13}C-, and ^{11}B-) were obtained at ambient temperature on Bruker DRX-400 or Bruker DRX-500 spectrometers. Chemical shifts are reported relative to $CHCl_3/CDCl_3$ (δ ^{1}H = 7.26 ppm, δ ^{13}C = 77.0 ppm) and external $Et_2O{\cdot}BF_3$ (δ ^{11}B = 0 ppm), respectively. Mass spectra were measured with a Bruker Daltonics Autoflex IITM MALDI-TOF MS spectrometer, Micromass GC-TOF for EI-MS (70 eV) and a ESI-MS (LCQ Fleet, Thermo Fisher Scientific). Melting points were measured with an X4 digital melting point displayer. Phosphorescence measurements were carried out using a Hitachi F-4600 fluorescence spectrophotometer. Electronic absorption spectra were recorded with Shimadzu UV-2550 spectrophotometers. Phosphorescence lifetimes were determined by an Edinburgh Instruments laser impulse fluorometer with picosecond time resolution. Elemental analyses for C, H and N were performed on a Vario MICRO elemental analyzer. IR data were collected on a Bruker Vacuum FT-IR Spectrometer 80 V. X-ray diffraction data were collected on a Bruker Smart CCD Apex DUO diffractometer with graphite monochromated Mo Kα radiation (λ = 0.71073 Å) using the ω–2θ scan mode.

Synthesis of 1a

A mixture of **a** (0.66 g, 2.2 mmol, 1.1 equiv), 2-(tributylstannyl) pyridine (0.74 g, 2 mmol), and $Pd(PPh_3)_4$ (0.23 g, 5% mmol) in dry toluene (40 mL) was refluxed for 24 h under argon atmosphere. After cooling down to room temperature, the solvent was evaporated under reduced pressure and the residue was purified by column chromatography on silica gel using ethylacetate/*n*-hexane (1 : 8, v/v) as eluent. Drying in vacuum afforded a yellowish white powder of **1a** (0.49 g, 83%).

^{1}H NMR ($CDCl_3$): δ 8.80 (d, J = 1.9 Hz, 1H), 8.69 (d, J = 4.2 Hz, 1H), 8.41 (m, 2H), 7.91 (dd, J = 2.2, 8.4 Hz, 1H), 7.85 (t, J = 7.6 Hz, 1H), 7.36 (m, 1H), 4.01 (s, 1H, carborane–CH), 3.40–1.71 (br, 10H, B–H). ^{13}C NMR ($CDCl_3$): δ 157.34, 154.47, 149.36, 147.79, 137.05, 136.13, 129.24, 124.45, 121.38, 120.45, 121.6 (py-C), 73.75 (B–C) and 60.19 (B–C). ^{11}B NMR ($CDCl_3$): δ 1.6 (1B), −0.6 (1B), −5.5 (2B), −7.7 (2B), −8.5 (2B) and −9.4 (2B). IR (KBr): (ν cm^{-1}) 2588. EI-MS (m/z): 298.20.

Synthesis of 1b

This compound was prepared in a manner analogous to the synthesis of **1a** using **b** (0.63 g, 2.0 mmol) and 2-(tributylstannyl) pyridine (1.10 g, 3 mmol), and $Pd(PPh_3)_4$ (0.12 g, 5% mmol) to afford a yellowish white powder of **1b** (0.51 g, 81%).

^{1}H NMR ($CDCl_3$): δ 8.94 (d, J = 2.4 Hz, 1H), 8.72 (d, J = 4.5 Hz, 1H), 8.46 (dd, J = 8.5, 7.8, 2H), 8.07 (dd, J = 2.6, 8.5 Hz, 1H), 7.87 (td, J = 1.7, 7.8 Hz, 1H), 7.38 (ddd, J = 1.1, 4.9, 7.6 Hz, 1H), 1.75 (s, 1H, carborane-CH_3), 3.40–1.61 (br, 10H, B–H). ^{13}C NMR ($CDCl_3$): δ 157.81, 154.50, 150.88, 149.44, 139.29, 137.09, 126.88, 124.55, 121.48, 120.54 (py-C), 78.93 (B–C) and 77.21 (B–C), and 23.20 (CH_3). ^{11}B NMR ($CDCl_3$): δ 0.6 (2B), −1.2 (2B), −6.3 (3B) and −6.7 (3B). IR (KBr): (ν cm^{-1}) 2588. EI-MS (m/z): 312.00.

Synthesis of 1c

This compound was prepared in a manner analogous to the synthesis of **1a** using **c** (0.38 g, 1.0 mmol) and 2-(tributylstannyl) pyridine (0.55 g, 1.5 mmol), and $Pd(PPh_3)_4$ (0.06 g, 5% mmol) to afford a yellowish white powder of **1c** (0.29 g, 76%).

^{1}H NMR ($CDCl_3$): δ 8.74 (d, J = 2.1 Hz, 1H), 8.65 (d, J = 4.2 Hz, 1H), 8.33 (d, J = 7.9, 1H), 8.22 (d, J = 8.5 Hz, 1H), 7.81 (m, 2H), 7.48 (m, 2H), 7.33 (dd, J = 5.1, 6.6 Hz, 1H), 7.25 (dd, J = 6.9, 7.3 Hz, 1H), 7.17 (dd, J = 4.8, 8.0 Hz, 2H), 3.40–1.80 (br, 10H, B–H). ^{13}C NMR ($CDCl_3$): δ 157.14, 154.48, 150.48, 149.27, 138.71, 137.04, 130.61, 130.09, 128.62, 126.80, 124.42, 121.44, 119.99, 85.22 (B–C) and 82.02 (B–C). ^{11}B NMR ($CDCl_3$): δ 0.9 (2B), −6.1 (3B), 6.9 (3B) and −8.6 (2B). IR (KBr): (ν cm^{-1}) 2596. EI-MS (m/z): 374.30.

Synthesis of 1d

This compound was prepared in a manner analogous to the synthesis of **1a** using **d** (0.52 g, 2.0 mmol) and 2-(tributylstannyl) pyridine (1.10 g, 3 mmol), and $Pd(PPh_3)_4$ (0.12 g, 5% mmol) to afford a yellowish white powder of **1d** (0.53 g, 90%). ^{1}H NMR ($CDCl_3$): δ 8.69 (d, J = 4.3 Hz, 1H), 8.67 (d, J = 5.2 Hz, 1H), 8.47 (d, J = 1.7 Hz, 1H), 8.43 (d, J = 7.9 Hz, 1H), 7.85 (td, J = 1.7, 7.8 Hz, 1H), 7.43 (dd, J = 2.1, 5.2 Hz, 1H), 7.37 (m, 1H), 4.24 (s, 1H, carborane-CH), 3.30–1.70 (br, 10H, B–H). ^{13}C NMR ($CDCl_3$): δ 157.03, 154.51, 150.88, 149.75, 149.18, 143.00, 137.07, 124.44, 121.83, 121.33, 118.02 (py-C), 74.04 (B–C) and 58.76 (B–C). ^{11}B NMR ($CDCl_3$): δ 1.4 (2B), −0.2 (1B), −5.4 (3B), −8.0 (2B) and −9.6 (2B). IR (KBr): (ν cm^{-1}) 2573. EI-MS (m/z): 298.20.

Synthesis of 1f

This compound was prepared in a manner analogous to the synthesis of **1a** using **f** (0.66 g, 2.0 mmol) and 2-(tributylstannyl) pyridine (1.10 g, 3 mmol), and $Pd(PPh_3)_4$ (0.12 g, 5% mmol) to afford a yellowish white powder of **1f** (0.61 g, 82%).

^{1}H NMR ($CDCl_3$): δ 8.70 (d, J = 4.1 Hz, 1H), 8.58 (d, J = 1.4 Hz, 1H), 8.44 (d, J = 5.2 Hz, 1H), 8.30 (d, J = 8.0 Hz, 1H), 7.80 (td, J = 1.9, 7.8 Hz, 1H), 7.51 (d, J = 7.3 Hz, 2H), 7.34 (dd, J = 5.3, 7.7 Hz, 1H), 7.23 (m, 2H), 7.16 (m, 2H), 3.40–1.80 (br, 10H, B–H). ^{13}C NMR ($CDCl_3$): δ 156.79, 154.67, 149.37, 140.03, 136.91, 130.56, 130.11, 128.60, 124.28, 124.04, 122.35, 121.11, 85.20 (B–C) and 82.32 (B–C). ^{11}B NMR ($CDCl_3$): δ 1.6 (2B), 0.7 (3B), −6.9 (3B) and −8.3 (2B). IR (KBr): (ν cm^{-1}) 2597. EI-MS (m/z): 373.20.

Synthesis of 1g

Sodium hydride (60% dispersion in mineral oil, 0.03 g, 0.75 mmol) was suspended in dry DMF (5 mL). After being cooled down to −20 °C, a solution of **1a** (0.21 g, 0.68 mmol) in DMF (5 mL) was slowly added to the suspension. The mixture was stirred at room temperature for 1 h, then 2-iodopropane (0.17, 1.0 mmol) was added at −20 °C, and further stirred at room temperature overnight. The reaction was quenched by saturated aqueous NH_4Cl solution, and extracted with diethyl ether (30 mL × 3). The organic layer was washed with water (30 mL × 3) and dried over $MgSO_4$. The solvent was evaporated under reduced pressure. The residue was purified by column chromatography on silica gel using ethylacetate/n-hexane (1 : 4, v/v) as eluent. Drying in vacuum afforded a pale yellow powder of **1g** (0.12 g, 51%).

^{1}H NMR ($CDCl_3$): δ 8.91 (d, J = 0.6 Hz, 1H), 8.72 (d, J = 3.5 Hz, 1H), 8.47 (t, J = 9.3 Hz, 2H), 8.05 (d, J = 8.7 Hz, 1H), 7.88 (t, J = 7.5 Hz, 1H), 7.39 (m, 1H), 3.50–1.80 (br, 10H, B–H), 1.73 (sept, 1H, J = 7.0 Hz, –$CHCH_3$), 1.09 (d, J = 7.0 Hz, 3H, –CH_3), 1.06 (d, J = 7.0 Hz, 3H, –CH_3). ^{13}C NMR ($CDCl_3$): δ 157.83, 154.48, 150.90, 149.41, 139.33, 137.04, 126.73, 124.52, 121.48, 120.52, 121.6 (py-C), 88.60 (B–C), 82.22 (B–C), 31.64, and 23.90 (isopropyl-C). ^{11}B NMR ($CDCl_3$): δ 0.4 (3B), −6.5 (4B) and −8.6 (3B). IR (KBr): (ν cm^{-1}) 2585. EI-MS (m/z): 340.10.

Synthesis of 1h

This compound was prepared in a manner analogous to the synthesis of **1g** using **1a** (0.24 g, 0.68 mmol) and 1-iodo-2-methylpropane (0.18 g, 1.0 mmol) to afford a yellowish white powder of **1h** (0.13 g, 54%).

^{1}H NMR ($CDCl_3$): δ 8.92 (s, 1H), 8.73 (s, 1H), 8.50 (d, J = 7.6 Hz, 2H), 8.05 (d, J = 8.7 Hz, 1H), 8.05 (d, J = 8.1 Hz, 1H), 7.91 (t, J = 6.7 Hz, 1H), 7.41 (m, 1H), 3.60–1.80 (br, 10H, B–H), 1.83–1.70 (m, 2H, –$CHCH_2$), 0.85 (d, J = 7.0 Hz, 6H, –CH_3). ^{13}C NMR ($CDCl_3$): δ 157.76, 154.52, 151.07, 149.41, 139.45, 137.14, 126.95, 124.57, 121.55, 120.52, 121.6 (py-C), 82.26 (B–C), 80.99 (B–C), 43.88, 28.43, and 23.30 (isobutyl-C). ^{11}B NMR ($CDCl_3$): δ −0.1 (3B), −6.6 (4B) and −7.5 (3B). IR (KBr): (ν cm^{-1}) 2591. EI-MS (m/z): 354.30.

Synthesis of 1e

This compound was prepared in a manner analogous to the synthesis of **1g** using **1d** (0.21 g, 0.68 mmol) and iodomethane (0.15 g, 1.0 mmol) to afford a yellowish white powder of **1e** (0.14 g, 63%).

^{1}H NMR ($CDCl_3$): δ 8.74 (d, J = 6.1 Hz, 1H), 8.44 (d, J = 7.9 Hz, 1H), 7.85 (t, J = 7.5 Hz, 2H), 7.55 (d, J = 3.4 Hz, 1H), 7.37 (m, 2H), 1.78 (s, 1H, CH_3), 3.50–1.71 (br, 10H, B–H). ^{13}C NMR ($CDCl_3$): δ 157.50, 154.79, 150.04, 149.49, 140.34, 137.14, 124.91, 124.53, 122.48, 121.21, 118.20 (py-C), 79.55 (B–C), 58.95 (B–C), and 23.44 (CH_3). ^{11}B NMR ($CDCl_3$): δ 0.9 (2B), −1.4 (2B), and −6.6 (6B). IR (KBr): (ν cm^{-1}) 2590. EI-MS (m/z): 311.20.

Synthesis of 1i

This compound was prepared in a manner analogous to the synthesis of **1g** using **1d** (0.21 g, 0.68 mmol) and 2-iodopropane (0.17, 1.0 mmol) to afford a yellowish white powder of **1i** (0.13 g, 58%).

^{1}H NMR ($CDCl_3$): δ 8.73 (s, 1H), 8.44 (d, J = 7.8 Hz, 1H), 7.86 (t, J = 7.2 Hz, 2H), 7.53 (d, J = 3.4 Hz, 1H), 7.38 (m, 2H), 3.50–1.71 (br, 10H, B–H), 1.76 (sept, J = 7.0 Hz, 1H, –$CHCH_3$), 1.09 (d, J = 7.0 Hz, 3H, –CH_3), 1.08 (d, J = 7.0 Hz, 3H, –CH_3). ^{13}C NMR ($CDCl_3$): δ 157.34, 154.64, 149.84, 149.38, 140.12, 136.96, 124.78, 124.36, 122.46, 121.25 (py-C), 88.58 (B–C), 82.51 (B–C), 31.82, and 24.02 (isopropyl-C). ^{11}B NMR ($CDCl_3$): δ 0.2 (3B), −6.4 (4B) and −8.4 (3B). IR (KBr): (ν cm^{-1}) 2595. EI-MS (m/z): 338.30.

Synthesis of 1j

This compound was prepared in a manner analogous to the synthesis of **1g** using **1d** (0.24 g, 0.68 mmol) and 1-iodo-2-methylpropane (0.18 g, 1.0 mmol) to afford a yellowish white powder of **1j** (0.13 g, 55%).

^{1}H NMR ($CDCl_3$): δ 8.73 (d, J = 5.0 Hz, 3H), 8.45 (d, J = 7.9 Hz, 1H), 7.86 (t, J = 8.4 Hz, 1H), 7.52 (dd, J = 1.9, 5.1 Hz, 1H), 7.38 (dd, J = 5.1, 6.8 Hz, 1H), 3.60–1.80 (br, 10H, B–H), 1.79–1.76 (m, 3H, –$CHCH_2$), and 0.84 (d, J = 7.0 Hz, 6H, –CH_3). ^{13}C NMR ($CDCl_3$): δ 157.31, 154.60, 149.82, 149.34, 140.19, 136.93, 124.78, 124.34, 122.50, 121.21 (py-C), 82.19 (B–C), 81.35 (B–C), 43.81, 28.39, and 23.23 (isobutyl-C). ^{11}B NMR ($CDCl_3$): δ 0.5 (2B), −0.3 (2B), −6.6 (3B), and −7.3 (3B). IR (KBr): (ν cm^{-1}) 2595. EI-MS (m/z): 353.20.

Synthesis of 4a

5-*o*-Carboranyl-2-bromopyridine (**a**) (1.30 g, 4.33 mmol) was charged into a flask which was evacuated and recharged by argon. Anhydrous *m*-xylene (35 mL) was injected by a syringe, followed by addition of hexa-*n*-butyldistannane (1.18 mL, 50 mol%). Argon was bubbled through the stirred solution for 1 h before $Pd(PPh_3)_4$ (0.12 g, 0.101 mmol) was added from a tip tube. The reaction mixture was heated to 130 °C for 3 days until all starting material was consumed, then poured into aqueous EDTA (1 M, 25 mL). After the mixture was stirred for 15 min, the phases were separated. The aqueous phase was extracted with chloroform, and the combined organic phases were dried over Na_2SO_4. After evaporation of the solvents, the crude product was flash chromatographed (alumina, 5 : 1 hexanes/ethylacetate) to afford **4a** as a white yellow solid (0.33 g, 35%).

^{1}H NMR ($CDCl_3$) δ (ppm): δ 8.82 (d, J = 2.3 Hz, 2H), 8.41 (d, J = 8.5 Hz, 2H), 7.95 (dd, J = 2.3, 8.5 Hz, 2H), 4.01 (s, 2H, carborane), 3.15–1.70 (br, 20H, B–H). ^{13}C NMR δ (ppm): 155.72, 147.98, 136.33, 130.02, 120.82, 73.46 (B–C) and 60.11 (B–C). ^{11}B NMR δ (ppm): 1.6 (2B), −0.5 (1B), −5.5 (3B), −7.7 (2B), −8.5 (1B) and −8.9 (1B). EI-MS (m/z): 440.20.

Synthesis of 2a

$[(dfppy)_2Ir(\mu\text{-}Cl)]_2$ (0.2432 g, 0.2 mmol), **1a** (0.14 g, 0.44 mmol) were dissolved in methanol (10 mL) and CH_2Cl_2 (10 mL). The resulting mixture was refluxed for 8 h under argon. After cooling down to room temperature, 10-fold excess of KPF_6 was added. The mixture was stirred for 2 h, and then filtered to remove insoluble inorganic salts. The resulting solution was evaporated to dryness under reduced pressure. The residue was chromatographed on silica gel with elution by PE/ethyl acetate 1 : 3 (v/v) to give **2a** as a yellow solid. Yield: 166 mg (41%).

^{1}H NMR (500 MHz, ^6d-acetone): 8.89 (m, 2H), 8.52 (dd, J = 2.3, 8.7 Hz, 1H), 8.37 (m, 3H), 8.26 (m, 3H), 8.07 (m, 3H), 7.97 (d, J = 5.5 Hz, 1H), 7.91 (d, J = 5.5 Hz, 1H), 7.22 (d, J = 6.2 Hz, 2H), 6.78 (m, 1H), 5.84 (dd, J = 2.2, 8.5 Hz, 2H), 5.15 (s, 1H, carborane-CH), 3.15–1.72 (br, 10H, BH). ^{13}C NMR (^6d-acetone): 156.87, 154.07, 150.89, 149.77, 149.67, 149.07, 140.06, 139.67, 139.48, 138.58, 133.17, 129.31, 125.78, 124.58, 124.09, 123.90, 123.42, 123.15, 113.61, 113.41, 98.96, 98.85, 71.63 (B–C) and 60.92 (B–C). ^{11}B NMR (^6d-acetone): −0.7 (2B), −0.5 (1B), −5.9 (3B), −8.1 (2B) and −9.5 (2B). $C_{34}H_{30}B_{10}N_4F_4IrPF_6$ calcd: C, 40.19; N, 5.51; H, 2.97. Found: C, 39.80; N, 4.97; H, 2.85. MALDI-TOF: [M − PF_6] (m/z) 871.832. IR (KBr): (ν cm^{-1}) 2589 (B–H). Melting point: 233–235 °C.

Synthesis of 2b

This compound was prepared in a manner analogous to the synthesis of **2a** using $[(dfppy)_2Ir(\mu\text{-}Cl)]_2$ (0.2432 g, 0.2 mmol) and **1b** (0.13 g, 0.44 mmol) to afford a yellow powder. Yield: 260 mg (63%).

^{1}H NMR (500 MHz, ^6d-acetone): 8.95 (d, J = 8.6 Hz, 2H), 8.63 (dd, J = 2.2, 8.7 Hz, 2H), 8.38 (m, 3H), 8.28 (m, 2H), 8.07 (m, 2H), 7.93 (d, J = 5.6 Hz, 1H), 7.81 (m, 1H), 7.22 (m, 2H), 6.92 (m, 1H), 6.79 (m, 1H), 5.87 (m, 2H), 3.25–1.70 (br, 10H, BH), 1.68 (s, 3H, –CH_3). ^{13}C NMR (^6d-acetone): 163.78, 163.68, 163.55, 163.46, 162.51, 162.14, 161.72, 161.63, 161.51, 161.41, 159.44, 159.33, 157.00, 153.32, 152.23, 150.29, 149.93, 149.17, 149.13, 139.09, 138.90, 125.38, 124.48, 123.54, 123.27, 113.01, 112.94, 112.88, 98.24, 98.03, 97.88, 97.67, 71.31 (B–C), 75.81 (B–C), and 21.47 (CH_3). ^{11}B NMR (^6d-acetone): 1.1 (2B), −1.6 (2B) and −6.8 (6B). $C_{35}H_{32}B_{10}F_4N_4IrPF_6$ calcd: C, 40.82; N, 5.44; H, 3.13. Found: C, 40.70; N, 5.17; H, 3.05. MALDI-TOF: [M − PF_6] (m/z) 885.258. IR (KBr): (ν cm^{-1}) 2587 (B–H). Melting point: 238–240 °C.

Synthesis of 2c

This compound was prepared in a manner analogous to the synthesis of **2a** using $[(dfppy)_2Ir(\mu\text{-}Cl)]_2$ (0.2432 g, 0.2 mmol) and **1c** (0.16 g, 0.44 mmol) to afford a yellow orange powder. Yield: 253 mg (58%).

^{1}H NMR (500 MHz, ^6d-acetone): 8.79 (d, J = 8.8 Hz, 2H), 8.51 (d, J = 8.5 Hz, 2H), 8.34 (d, J = 8.3 Hz, 2H), 8.17 (m, 3H), 8.02 (m, 2H), 7.78 (m, 2H), 7.34 (m, 5H), 7.15 (d, J = 5.4 Hz, 2H), 7.00 (d, J = 9.0 Hz, 1H), 6.77 (d, J = 8.9 Hz, 1H), 5.78 (d, J = 5.9 Hz, 2H), 3.20–1.80 (br, 10H, BH). ^{13}C NMR (^6d-acetone): 163.03, 162.94,

163.55, 157.55, 154.10, 154.01, 153.90, 153.24, 153.15, 151.05, 149.96, 149.29, 142.34, 140.32, 140.10, 139.79, 131.57, 130.38, 129.76, 129.10, 128.80, 126.31, 124.97, 124.36, 123.90, 123.66, 123.42, 114.30, 114.07, 113.85, 113.61, 99.06, 98.83, 98.70, 98.47, 85.74 (B–C) and 79.40 (B–C). ^{11}B NMR (^{6}d-acetone): 1.7 (2B), −0.4 (2B) and −7.2 (6B). $C_{40}H_{34}B_{10}F_4N_4IrPF_6$. Calcd: C, 43.99; N, 5.13; H, 3.14. Found: C, 43.60; N, 5.01; H, 3.02. MALDI-TOF: [M − PF_6] (m/z) 947.185. IR (KBr): (ν cm^{-1}) 2586 (B–H). Melting point: 237–239 °C.

Synthesis of 2d

This compound was prepared in a manner analogous to the synthesis of **2a** using [(dfppy)$_2$Ir(μ-Cl)]$_2$ (0.2432 g, 0.2 mmol) and **1g** (0.15 g, 0.44 mmol) to afford a yellow powder. Yield: 267 mg (63%).

^{1}H NMR (500 MHz, ^{6}d-acetone): 8.95 (d, J = 8.5 Hz, 2H), 8.62 (dd, J = 2.3, 8.7 Hz, 2H), 8.39 (m, 3H), 8.28 (t, J = 4.2 Hz, 2H), 8.08 (m, 2H), 8.03 (d, J = 5.6 Hz, 1H), 7.93 (d, J = 5.3 Hz, 1H), 7.81 (m, 1H), 7.23 (m, 2H), 6.93 (m, 1H), 6.79 (m, 1H), 5.85 (m, 1H), 3.20–1.80 (br, 10H, BH), 1.64 (sept, J = 7.0 Hz, 1H, –$CHCH_3$), 0.90 (d, J = 7.0 Hz, 3H, –CH_3), 0.87 (d, J = 7.0 Hz, 3H, –CH_3). ^{13}C NMR (^{6}d-acetone): 163.86, 163.76, 163.61, 163.51, 162.65, 162.59, 162.18, 162.13, 161.81, 161.72, 161.57, 161.41, 159.49, 159.40, 159.34, 157.08, 153.42, 153.31, 152.31, 152.26, 150.34, 149.81, 149.18, 149.06, 139.10, 138.98, 128.87, 125.46, 124.66, 123.27, 112.99, 112.85, 98.30, 98.09, 97.87, 97.71, 88.58 (B–C), 78.84 (B–C), 30.78, 22.32 and 22.06. ^{11}B NMR (^{6}d-acetone): 0.1 (3B), −6.7 (4B) and −8.4 (3B). $C_{37}H_{36}B_{10}F_4N_4IrPF_6$. Calcd: C, 42.00; N, 5.30; H, 3.43. Found: C, 41.60; N, 5.01; H, 3.22. MALDI-TOF: [M − PF_6] (m/z) 921.135. IR (KBr): (ν cm^{-1}) 2588 (B–H). Melting point: 236–237 °C.

Synthesis of 2e

This compound was prepared in a manner analogous to the synthesis of **2a** using [(dfppy)$_2$Ir(μ-Cl)]$_2$ (0.2432 g, 0.2 mmol) and **1h** (0.16 g, 0.44 mmol) to afford a yellow powder. Yield: 240 mg (56%).

^{1}H NMR (500 MHz, ^{6}d-acetone): 8.95 (d, J = 8.5 Hz, 2H), 8.65 (dd, J = 2.3, 8.7 Hz, 2H), 8.40 (m, 3H), 8.28 (dd, J = 3.5, 11.7 Hz, 2H), 8.10 (m, 1H), 8.03 (d, J = 5.6 Hz, 1H), 7.98 (d, J = 5.3 Hz, 1H), 7.82 (m, 1H), 7.27 (m, 1H), 7.20 (ddd, J = 1.2, 6.0, 7.3 Hz, 1H), 6.93 (m, 1H), 6.79 (m, 1H), 5.86 (dd, J = 2.3, 8.4 Hz, 2H), 3.10–1.80 (br, 10H, BH), 0.90–0.82 (m, 3H, –$CHCH_2$), 0.72 (d, J = 7.0 Hz, 3H, –CH_3), 0.66 (d, J = 7.0 Hz, 3H, –CH_3). ^{13}C NMR (^{6}d-acetone): 163.36, 162.95, 157.79, 154.04, 153.02, 151.13, 150.74, 149.98, 149.71, 139.91, 139.69, 129.63, 126.17, 125.27, 123.95, 113.71, 113.58, 99.05, 98.83, 98.64, 98.43, 82.74 (B–C), 78.17 (B–C), 43.16, 22.22 and 22.07. ^{11}B NMR (^{6}d-acetone): 0.9 (2B), −0.6 (2B) and −6.9 (6B). $C_{38}H_{38}B_{10}F_4N_4IrPF_6$. Calcd: C, 42.00; N, 5.29; H, 3.43. Found: C, 41.50; N, 5.11; H, 3.21. MALDI-TOF: [M − PF_6] (m/z) 926.260. IR (KBr): (ν cm^{-1}) 2589 (B–H). Melting point: 236–238 °C.

Synthesis of 3a

This compound was prepared in a manner analogous to the synthesis of **2a** using [(dfppy)$_2$Ir(μ-Cl)]$_2$ (0.2432 g, 0.2 mmol) and **1d** (0.14 g, 0.44 mmol) to afford a yellow powder. Yield: 174 mg (43%).

^{1}H NMR (500 MHz, ^{6}d-acetone): 9.06 (d, J = 8.2 Hz, 2H), 8.91 (d, J = 1.8 Hz, 1H), 8.36 (m, 3H), 8.25 (dd, J = 5.6, 12.1 Hz, 2H), 8.06 (dd, J = 8.3, 19.3 Hz, 2H), 7.95 (dd, J = 2.1, 5.9 Hz, 1H), 7.90 (dd, J = 5.7, 10.3 Hz, 2H), 7.79 (m, 1H), 7.24 (m, 1H), 7.18 (m, 1H), 6.77 (m, 1H), 5.79 (dd, J = 2.3, 8.5 Hz, 1H), 5.74 (dd, J = 2.3, 8.6 Hz, 1H), 5.48 (s, 1H, carborane CH), 3.10–1.75 (br, 10H, BH). ^{13}C NMR (^{6}d-acetone): 164.23, 163.46, 163.41, 163.35, 162.18, 162.07, 160.10, 160.00, 156.72, 154.58, 153.70, 153.65, 153.60, 151.21, 150.89, 149.64, 149.58, 145.02, 139.85, 139.64, 139.58, 129.28, 127.17, 125.74, 123.87, 122.42, 113.42, 113.39, 113.24, 98.84, 98.79, 98.62, 98.41, 98.36, 73.08 (B–C) and 59.73 (B–C). ^{11}B NMR (^{6}d-acetone): 0.6 (2B), −5.4 (3B), −7.9 (3B) and −9.5 (2B). $C_{34}H_{30}B_{10}N_4F_4IrPF_6$ calcd: C, 40.19; N, 5.51; H, 2.97. Found: C, 40.07; N, 5.37; H, 2.89. MALDI-TOF: [M − PF_6] (m/z) 873.396. IR (KBr): (ν cm^{-1}) 2594 (B–H). Melting point: 230–232 °C.

Synthesis of 3b

This compound was prepared in a manner analogous to the synthesis of **2a** using [(dfppy)$_2$Ir(μ-Cl)]$_2$ (0.2432 g, 0.2 mmol) and **1e** (0.14 g, 0.44 mmol) to afford a yellow powder. Yield: 263 mg (64%).

^{1}H NMR (500 MHz, ^{6}d-acetone): 9.17 (d, J = 8.2 Hz, 1H), 8.98 (d, J = 1.9 Hz, 1H), 8.37 (dd, J = 3.4, 5.9 Hz, 3H), 8.25 (d, J = 5.3 Hz, 1H), 8.07 (m, 3H), 7.91 (dd, J = 6.1, 9.4 Hz, 2H), 7.80 (m, 2H), 7.20 (m, 2H), 6.78 (m, 2H), 5.77 (dd, J = 2.3, 8.5 Hz, 2H), 3.15–1.70 (br, 10H, BH), 1.92 (s, 3H, –CH_3). ^{13}C NMR (^{6}d-acetone): 163.25, 163.20, 163.16, 163.11, 162.01, 161.91, 156.97, 154.45, 153.60, 153.55, 153.47, 151.43, 150.58, 149.69, 149.59, 139.76, 139.41, 126.07, 125.97, 123.85, 123.80, 113.35, 113.27, 113.13, 98.70, 98.65, 98.49, 98.44, 98.27, 98.22, 78.45 (B–C), 77.84 (B–C) and 22.24 (CH_3). ^{11}B NMR (^{6}d-acetone): 0.9 (2B), −1.8 (2B), and −6.7 (6B). $C_{35}H_{32}B_{10}F_4N_4IrPF_6$ calcd: C, 40.82; N, 5.44; H, 3.13. Found: C, 40.71; N, 5.27; H, 3.01. MALDI-TOF: [M − PF_6] (m/z) 887.635. IR (KBr): (ν cm^{-1}) 2589 (B–H). Melting point: 232–234 °C.

Synthesis of 3c

This compound was prepared in a manner analogous to the synthesis of **2a** using [(dfppy)$_2$Ir(μ-Cl)]$_2$ (0.2432 g, 0.2 mmol) and **1f** (0.16 g, 0.44 mmol) to afford a yellow powder. Yield: 240 mg (55%).

^{1}H NMR (500 MHz, ^{6}d-acetone): 8.98 (d, J = 7.7 Hz, 1H), 8.70 (d, J = 5.8 Hz, 1H), 8.34 (dd, J = 7.5, 14.7 Hz, 3H), 8.10 (m, 4H), 7.77 (m, 3H), 7.58 (d, J = 8.0 Hz, 3H), 7.38 (t, J = 7.4, 1H), 7.22 (m, 4H), 6.75 (t, J = 7.7 Hz, 2H), 5.70 (ddd, J = 1.8, 8.5, 10.8 Hz, 2H), 3.10–1.80 (br, 10H, BH). ^{13}C NMR (^{6}d-acetone): 163.71, 162.75, 162.58, 161.57, 159.53, 155.80, 153.53, 153.08, 152.77, 150.34, 150.23, 148.68, 148.54, 139.49, 139.16, 129.99, 128.08, 123.29, 122.82, 112.95, 112.82, 98.24, 98.05, 85.33 (B–C) and 79.94 (B–C). ^{11}B NMR (^{6}d-acetone): 1.9 (2B), −0.4 (2B) and −6.9 (6B). $C_{40}H_{34}B_{10}F_4N_4IrPF_6$. Calcd: C, 43.99; N, 5.13; H, 3.14. Found: C, 43.58; N, 5.00; H, 3.03. MALDI-TOF: [M − PF_6] (m/z)

949.685. IR (KBr): (ν cm^{-1}) 2590 (B–H). Melting point: 231–233 °C.

Synthesis of 3d

This compound was prepared in a manner analogous to the synthesis of **2a** using $[(dfppy)_2Ir(\mu\text{-}Cl)]_2$ (0.2432 g, 0.2 mmol) and **1i** (0.15 g, 0.44 mmol) to afford a yellow powder. Yield: 262 mg (62%).

^{1}H NMR (500 MHz, ^6d-acetone): 9.15 (d, J = 8.2 Hz, 1H), 8.94 (d, J = 1.7 Hz, 1H), 8.36 (m, 3H), 8.22 (d, J = 5.2 Hz, 1H), 8.06 (m, 4H), 7.88 (t, J = 6.5 Hz, 2H), 7.79 (m, 1H), 7.20 (m, 2H), 6.77 (m, 2H), 5.76 (ddd, J = 2.3, 8.5, 16.6 Hz, 2H), 3.10–1.70 (br, 10H, BH), 1.95 (sept, J = 7.0 Hz, 1H, –$CHCH_3$), 1.05 (d, J = 7.0 Hz, 3H, –CH_3), 1.01 (d, J = 7.0 Hz, 3H, –CH_3). ^{13}C NMR (^6d-acetone): 163.69, 163.61, 162.70, 161.66, 161.55, 161.44, 159.47, 159.37, 156.61, 153.93, 153.01, 151.05, 150.13, 149.18, 149.05, 139.38, 139.01, 125.56, 125.51, 123.32, 122.69, 113.02, 112.86, 112.71, 98.24, 98.02, 97.81, 89.27 (B–C), 80.28 (B–C), 31.09, 27.68 and 22.58. ^{11}B NMR (^6d-acetone): 0.1 (3B), −6.7 (4B) and −8.4 (3B). $C_{37}H_{36}B_{10}F_4N_4IrPF_6$. Calcd: C, 42.00; N, 5.30; H, 3.43. Found: C, 41.60; N, 5.11; H, 3.26. MALDI-TOF: [M − PF_6] (m/z) 915.525. IR (KBr): (ν cm^{-1}) 2581 (B–H). Melting point: 235–237 °C.

Synthesis of 3e

This compound was prepared in a manner analogous to the synthesis of **2a** using $[(dfppy)_2Ir(\mu\text{-}Cl)]_2$ (0.2432 g, 0.2 mmol) and **1j** (0.16 g, 0.44 mmol) to afford a yellow powder. Yield: 231 mg (54%).

^{1}H NMR (500 MHz, ^6d-acetone): 9.17 (d, J = 8.2 Hz, 1H), 8.98 (s, 1H), 8.38 (m, 3H), 8.24 (d, J = 5.1 Hz, 1H), 8.07 (m, 3H), 7.92 (dd, J = 5.5, 5.4 Hz, 3H), 7.80 (m, 2H), 7.23 (t, J = 6.2 Hz, 1H), 7.17 (t, J = 6.6 Hz, 1H), 6.78 (m, 1H), 5.78 (ddd, J = 2.2, 5.8, 8.2 Hz, 2H), 3.15–1.80 (br, 10H, BH), 1.90–1.62 (m, 3H, –$CHCH_2$), 0.73 (d, J = 7.0 Hz, 3H, –CH_3), 0.70 (d, J = 7.0 Hz, 3H, –CH_3). ^{13}C NMR (^6d-acetone): 164.27, 164.18, 163.32, 163.27, 162.24, 162.14, 160.02, 159.95, 157.09, 154.43, 153.62, 153.57, 153.51, 153.47, 151.54, 150.76, 149.66, 149.53, 141.63, 139.89, 139.58, 130.07, 129.26, 126.27, 126.05, 123.96, 123.76, 123.26, 113.59, 113.46, 113.32, 98.78, 98.56, 98.35, 83.28 (B–C), 79.48 (B–C), 43.14, 27.99 and 22.04. ^{11}B NMR (^6d-acetone): 0.7 (2B), −0.7 (2B) and −6.8 (6B). $C_{38}H_{38}B_{10}F_4N_4IrPF_6$. Calcd: C, 42.00; N, 5.29; H, 3.43. Found: C, 41.60; N, 5.01; H, 3.11. MALDI-TOF: [M − PF_6] (m/z) 929.514. IR (KBr): (ν cm^{-1}) 2583 (B–H). Melting point: 236–237 °C.

Synthesis of 4

This compound was prepared in a manner analogous to the synthesis of **2a** using $[(dfppy)_2Ir(\mu\text{-}Cl)]_2$ (0.2432 g, 0.2 mmol) and **4a** (0.19 g, 0.44 mmol) to afford a yellow powder. Yield: 240 mg (52%).

^{1}H NMR (500 MHz, ^6d-acetone): 8.94 (d, J = 8.5 Hz, 2H), 8.54 (d, J = 8.3 Hz, 2H), 8.42 (d, J = 8.4 Hz, 2H), 8.28 (d, J = 1.6 Hz, 2H), 8.09 (t, J = 7.8 Hz, 2H), 7.98 (d, J = 5.4 Hz, 2H), 6.91 (m, 4H), 5.91 (dd, J = 2.2, 8.4 Hz, 2H), 5.18 (s, 2H, carborane CH), 3.02–1.60 (br, 20H, BH). ^{13}C NMR (^6d-acetone): 163.63, 163.54, 162.26, 162.22, 161.92, 161.84, 161.50, 161.42, 159.78, 159.69, 155.00, 152.17, 152.13, 149.49, 148.67, 139.30, 138.30, 133.31, 127.15, 125.07, 123.66, 122.88, 113.40, 98.45, 98.27, 98.09, 70.96 (B–C) and 60.40 (B–C). ^{11}B NMR (^6d-acetone): 0.9 (4B), 0.1 (2B), −5.7 (6B), −8.2 (4B), and −9.3 (4B). $C_{36}H_{40}B_{20}N_4F_4IrPF_6$ calcd: C, 37.33; N, 4.84; H, 3.48. Found: C, 37.01; N, 4.67; H, 3.31. MALDI-TOF: [M − PF_6] (m/z) 1013.225. IR (KBr): (ν cm^{-1}) 2589 (B–H). Melting point: 245–247 °C.

Acknowledgements

We acknowledge the financial support from the National Natural Science Foundation of China (21531004, 21472086, 21271102), National Program for Support of Top-Notch Young Professionals, and high-performance computational center of Nanjing University.

Notes and references

1 D. G. Drubin and W. J. Nelson, *Cell*, 1996, **84**, 335.
2 (*a*) Y. D. Zhuang, P. Y. Chiang, C. W. Wang and K. T. Tan, *Angew. Chem., Int. Ed.*, 2013, **52**, 8124; (*b*) L. Huang and S. W. Tam-Chang, *J. Fluoresc.*, 2011, **21**, 213.
3 H. B. Xiao, P. Li, W. Zhang and B. Tang, *Chem. Sci.*, 2016, **7**, 1588.
4 (*a*) Z. G. Yang, J. F. Cao, Y. X. He, J. H. Yang, T. Kim, X. J. Peng and J. S. Kim, *Chem. Soc. Rev.*, 2014, **43**, 4563; (*b*) H. Zhu, J. L. Fan, J. J. Du and X. J. Peng, *Acc. Chem. Res.*, 2016, **49**, 2115.
5 (*a*) N. Jiang, J. L. Fan, F. Xu, X. J. Peng, H. Y. Mu, J. Y. Wang and X. Q. Xiong, *Angew. Chem., Int. Ed.*, 2015, **54**, 2510; (*b*) E. Yamaguchi, C. G. Wang, A. Fukazawa, M. Taki, Y. Sato, T. Sasaki, M. Ueda, N. Sasaki, T. Higashiyama and S. Yamaguchi, *Angew. Chem., Int. Ed.*, 2015, **54**, 4539; (*c*) C. G. Wang, A. Fukazawa, M. Taki, Y. Sato, T. Higashiyama and S. Yamaguchi, *Angew. Chem., Int. Ed.*, 2015, **54**, 15213.
6 M. Chen, Y. Q. Wu, Y. Liu, H. R. Yang, Q. Zhao and F. Y. Li, *Biomaterials*, 2014, **35**, 8748.
7 (*a*) Q. Zhao, F. Y. Li and C. H. Huang, *Chem. Soc. Rev.*, 2010, **39**, 3007; (*b*) Q. Zhao, C. H. Huang and F. Y. Li, *Chem. Soc. Rev.*, 2011, **40**, 2508; (*c*) Y. M. Yang, Q. Zhao, W. Feng and F. Y. Li, *Chem. Rev.*, 2013, **113**, 192; (*d*) X. L. Yang, G. J. Zhou and W. Y. Wong, *Chem. Soc. Rev.*, 2015, **44**, 8484; (*e*) W. Lv, T. Yang, Q. Yu, Q. Zhao, K. Zhang, H. Liang, S. Liu, F. Li and W. Huang, *Adv. Sci.*, 2015, **2**, 1500107; (*f*) H. Sun, S. Liu, W. Lin, K. Y. Zhang, W. Lv, X. Huang, F. Huo, H. Yang, G. Jenkins, Q. Zhao and W. Huang, *Nat. Commun.*, 2014, **5**, 3601; (*g*) W. Y. Wong and C. L. Ho, *Coord. Chem. Rev.*, 2009, **253**, 1709; (*h*) X. B. Xu, X. L. Yang, J. Zhao, G. J. Zhou and W. Y. Wong, *Asian J. Org. Chem.*, 2015, **4**, 394; (*i*) X. J. Liu, S. M. Wang, B. Yao, B. H. Zhang, C. L. Ho, W. Y. Wong, Y. X. Cheng and Z. Y. Xie, *Org. Electron.*, 2015, **21**, 1.
8 (*a*) R. N. Grimes, in *Carboranes*, Academic Press Inc, 2nd edn, 2011, vol. 9, p. 301; (*b*) B. P. Dash, R. Satapathy, J. A. Maguire and N. S. Hosmane, *New J. Chem.*, 2011, **35**, 1955; (*c*) B. P. Dash, R. Satapathy, E. R. Gaillard, J. A. Maguire and N. S. Hosmane, *J. Am. Chem. Soc.*, 2010, **132**, 6578; (*d*)

A. Ferrer-Ugalde, A. Gonzalez-Campo, C. Vinas, J. Rodriguez-Romero, R. Santillan, N. Farfan, R. Sillanpaa, A. Sousa-Pedrares, R. Nunez and F. Teixidor, *Chem.–Eur. J.*, 2014, **20**, 9940; (*e*) F. Teixidor, R. Nunez, C. Vinas, R. Sillanpaa and R. Kivekas, *Angew. Chem., Int. Ed.*, 2000, **39**, 4290; (*f*) R. Nunez, P. Farras, F. Teixidor, C. Vinas, R. Sillanpaa and R. Kivekas, *Angew. Chem., Int. Ed.*, 2006, **45**, 1270; (*g*) N. S. Hosmane, *Boron Science: New Technologies and Applications*, CRC Press, Boca Raton, FL, 2011; (*h*) N. S. Hosmane, *Boron and Gadolinium Neutron, Capture Therapy for Cancer Treatment*, World Scientific Publishers, Hackensack, NJ, USA, 2012, vol. 36, ch. 28, pp. 877–900; (*i*) V. I. Bregadze, *Chem. Rev.*, 1992, **92**, 209; (*j*) D. Zhao and Z. W. Xie, *Coord. Chem. Rev.*, 2016, **314**, 14; (*k*) A. Ferrer-Ugalde, E. J. Juarez-Perez, F. Teixidor, C. Vinas, R. Sillanpaa, E. Perez-Inestrosa and R. Nunez, *Chem.–Eur. J.*, 2012, **18**, 544; (*l*) J. X. Guo, D. Q. Liu, J. H. Zhang, J. J. Zhang, Q. Miao and Z. W. Xie, *Chem. Commun.*, 2015, **51**, 12004.

9 (*a*) Y. H. Lee, J. Park, J. Lee, S. U. Lee and M. H. Lee, *J. Am. Chem. Soc.*, 2015, **137**, 8018; (*b*) T. Kim, H. Kim, K. M. Lee, Y. S. Lee and M. H. Lee, *Inorg. Chem.*, 2013, **52**, 160; (*c*) H. J. Bae, J. Chung, H. Kim, J. Park, K. M. Lee, T. W. Koh, Y. S. Lee, S. Yoo, Y. Do and M. H. Lee, *Inorg. Chem.*, 2014, **53**, 128; (*d*) C. Shi, H. B. Sun, Q. B. Jiang, Q. Zhao, J. X. Wang, W. Huang and H. Yan, *Chem. Commun.*, 2013, **49**, 4746; (*e*) C. Shi, D. S. Tu, Q. Yu, H. Liang, Y. H. Liu, Z. H. Li, H. Yan, Q. Zhao and W. Huang, *Chem.–Eur. J.*, 2014, **20**, 16550; (*f*) X. Li, H. Yan and Q. Zhao, *Chem.–Eur. J.*, 2016, **22**, 1888.

10 (*a*) K. R. Wee, W. S. Han, D. W. Cho, S. Kwon, C. Pac and S. O. Kang, *Angew. Chem., Int. Ed.*, 2012, **51**, 2677; (*b*) C. Shi, H. B. Sun, X. Tang, W. Lv, H. Yan, Q. Zhao, J. X. Wang and W. Huang, *Angew. Chem., Int. Ed.*, 2013, **52**, 13434; (*c*) K. Kokado and Y. Chujo, *J. Org. Chem.*, 2011, **76**, 316; (*d*) K. Kokado, M. Tominaga and Y. Chujo, *Macromol. Rapid Commun.*, 2010, **31**, 1389; (*e*) S. Y. Kim, Y. J. Cho, G. F. Jin, W. S. Han, H. J. Son, D. W. Cho and S. O. Kang, *Phys. Chem. Chem. Phys.*, 2015, **17**, 15679; (*f*) K. Nishino, H. Yamamoto, K. Tanaka and Y. Chujo, *Org. Lett.*, 2016, **18**, 4064.

11 (*a*) Y. H. Lee, J. Park, S. J. Jo, M. Kim, J. Lee, S. U. Lee and M. H. Lee, *Chem.–Eur. J.*, 2015, **21**, 2052; (*b*) J. Park, Y. H. Lee, J. Y. Ryu, J. Lee and M. H. Lee, *Dalton Trans.*, 2016, **45**, 5667.

12 X. Li, X. Tong, H. Yan, C. S. Lu, Q. Zhao and W. Huang, *Chem.–Eur. J.*, 2016, **22**, 17282.

13 (*a*) J. V. Caspar and T. J. Meyer, *Inorg. Chem.*, 1983, **22**, 2444; (*b*) J. S. Wilson, N. Chawdhury, M. R. A. Al-Mandhary, M. Younus, M. S. Khan, P. R. Raithby, A. Kohler and R. H. Friend, *J. Am. Chem. Soc.*, 2001, **123**, 9412.

14 (*a*) M. Sarma, T. Chatterjee, R. Bodapati, K. N. Krishnakanth, S. Hamad, S. V. Rao and S. K. Das, *Inorg. Chem.*, 2016, **55**, 3530; (*b*) L. Zhu, X. Tang, Q. Yu, W. Lv, H. Yan, Q. Zhao and W. Huang, *Chem.–Eur. J.*, 2015, **21**, 4721.

15 (*a*) H. A. Al-Attar, G. C. Griffiths, T. N. Moore, M. Tavasli, M. A. Fox, M. R. Bryce and A. P. Monkman, *Adv. Funct. Mater.*, 2011, **21**, 2376; (*b*) E. M. Kober, B. P. Sullivan and T. J. Meyer, *Inorg. Chem.*, 1984, **23**, 2098; (*c*) A. P. Wilde and R. J. Watts, *J. Phys. Chem.*, 1991, **95**, 622.

16 (*a*) D. R. Green and J. C. Reed, *Science*, 1998, **281**, 1309; (*b*) H. Yoshida, Y. Y. Kong, R. Yoshida, A. J. Elia, A. Hakem, R. Hakem, J. M. Penninger and T. W. Mak, *Cell*, 1998, **94**, 739.

17 (*a*) G. Kroemer and J. C. Reed, *Nat. Med.*, 2000, **6**, 513; (*b*) T. Xiao, J. K. Fan, H. L. Huang, J. F. Gu, L. Y. Li and X. Y. Liu, *Cell Res.*, 2010, **20**, 367; (*c*) S. L. Luo, X. Tan, S. T. Fang, Y. Wang, T. Liu, X. Wang, Y. Yuan, H. Q. Sun, Q. R. Qi and C. M. Shi, *Adv. Funct. Mater.*, 2016, **26**, 2826.